



Journal of Applied and Computational Mechanics



Research Paper

Forced-based Shear-flexure-interaction Frame Element for Nonlinear Analysis of Non-ductile Reinforced Concrete Columns

Worathep Sae-Long¹, Suchart Limkatanyu², Chayanon Hansapinyo³, Thanongsak Imjai⁴,
Minho Kwon⁵

¹ Department of Civil Engineering, School of Engineering, University of Phayao, Phayao, 56000, Thailand, Email: s.worathep@yahoo.com

² Department of Civil Engineering, Faculty of Engineering, Prince of Songkla University, Songkhla, 90112, Thailand, Email: suchart.l@psu.ac.th

³ Center of Excellence in Natural Disaster Management, Department of Civil Engineering, Chiang Mai University, Chiang Mai, 50200, Thailand, Email: chayanon@eng.cmu.ac.th

⁴ School of Engineering and Resources, Walailak University, Nakhorn Si Thammarat, 80160, Thailand, Email: thanongsak.im@wu.ac.th

⁵ Department of Civil Engineering, ERI, Gyeongsang National University, Jinju, 660-701, South Korea, Email: kwonm@gnu.ac.kr

Received February 25 2020; Revised April 13 2020; Accepted for publication April 13 2020.

Corresponding author: Suchart Limkatanyu (suchart.l@psu.ac.th)

© 2020 Published by Shahid Chamran University of Ahvaz

Abstract. An efficient frame model with inclusion of shear-flexure interaction is proposed here for nonlinear analyses of columns commonly present in reinforced concrete (RC) frame buildings constructed prior to the introduction of modern seismic codes in the Seventies. These columns are usually characterized as flexure-shear critical RC columns with light and non-seismically detailed transverse reinforcement. The proposed frame model is developed within the framework of force-based finite element formulation and follows the Timoshenko beam kinematics hypothesis. In this type of finite element formulation, the internal force fields are related to the element force degrees of freedom through equilibrated force shape functions and there is no need for displacement shape functions, thus eliminating the problem of displacement-field inconsistency and resulting in the locking-free Timoshenko frame element. The fiber-section model is employed to describe axial and flexural responses of the RC section. The modified Mergos-Kappos interaction procedure and the UCSD shear-strength model form the core of the shear-flexure interaction procedure adopted in the present work. Capability, accuracy, and efficiency of the proposed frame element are validated and assessed through correlation studies between experimental and numerical responses of two flexure-shear critical columns under cyclic loadings. Distinct response characteristics inherent to the flexure-shear critical column can be captured well by the proposed frame model. The computational efficiency of the force-based formulation is demonstrated by comparing local and global responses simulated by the proposed force-based frame model with those simulated by the displacement-based frame model.

Keywords: Timoshenko frame element, Shear-flexure interaction, Fiber frame element, Seismic nonlinear analysis, Forced-based formulation, Flexure-shear critical column.

1. Introduction

Reinforced concrete (RC) has been widely used as construction material for several engineering structures due to its low cost but high efficiency [1]. Especially in developing countries, most of frame structures have been constructed by RC materials. Columns in RC frame structures are often regarded as the most critical load-bearing component and their losses of load-bearing capacities can lead to severe structural damages or even collapses of whole structures. Therefore, seismic responses of columns are critical to good performance of RC frame buildings during an earthquake event. However, a large stock of existing RC frame buildings had been constructed prior to the mid-1970s. As a result, these RC frame buildings fail to meet modern seismic codes and their columns are typically considered as “non-ductile” columns with inadequate and non-seismically detailed transverse reinforcement [2]. As evidenced in post-earthquake reconnaissance [3-6], these columns experienced severe damage and performed unsatisfactorily during the seismic events. Several researchers have conducted both experimental and computational research work to characterize behaviors of this column type [7-13]. The strong coupling between sectional shear and flexural actions has been confirmed by many experimental evidences to be a key factor to characterize behaviors of this column type [14-16]. It has been observed that shear strength capacity of the column section was degraded within the plastic hinge regions even though the transverse reinforcement did not reach the yielding state and the shear failure was triggered subsequent to flexural yielding of the column section. Biskinis et al. [17] defined this column type as the “flexure-shear” critical column. The diagnosis of the detriment of inelastic flexural deformations on the column-section shear strength is associated with the reduction in the concrete shear-strength contribution triggered by aggregate interlocking. This shear-transfer mechanism is jeopardized by opening of flexural-shear cracks caused by inelastic flexural deformations within the plastic-hinge region. Several researchers



have proposed various flexural deformation-dependent shear strength models to account for the sectional shear-flexure coupling effect [18-19].

Along with advances in computer technology, a nonlinear frame model has become more and more popular among structural engineers and plays a crucial role in analyzing, designing, and assessing both existing and newly constructed structures under extreme loadings (e.g. destructive earthquakes). This is especially necessary with the recently adopted performance-based design and assessment methodology [20]. Therefore, the nonlinear frame model can be used as an effective tool to quantify seismic-risk level of existing non-seismic designed RC frame buildings for upcoming seismic events. This is crucial to prioritization procedure in seismic rehabilitation programs since it is impossible to rehabilitate all existing non-seismic designed buildings to meet current seismic design codes due to economical limitation and service interruption. However, a standard nonlinear frame model considering only inelastic flexural actions cannot be used to characterize the seismic performance of flexure-shear critical columns in existing non-seismic designed frame buildings due to lack of sectional shear-flexure coupling effects. Therefore, an efficient nonlinear frame model capable of interacting shear with flexural actions, accounting for inelastic shear responses, and identifying failure modes is required and this is the main focus of the present work.

In order to incorporate shear actions into nonlinear frame models for seismic analyses of RC frame structures, a diversity of frame models have been proposed by several researchers with various degrees of complexities. As discussed in the state-of-the-art report by Ceresa et al. [21-22], nonlinear frame models considering shear actions can be categorized into two groups, namely: the non-distributed inelastic frame model and the distributed inelastic frame model.

The first group accounts for shear actions by introducing shear-springs at member ends [23-27] and is often referred to as the "non-distributed" inelastic frame model. However, this model type can represent inelastic responses only at member ends, thus failing to capture gradual spread inelasticity.

To remedy the limitation inherent to the first group, the second group introduces inelastic responses within the plastification zone (plastic-hinge length) or injects inelastic responses into the model at the section level. As a result, this model type is often referred to as the "distributed" inelastic frame model. Due to the salient feature of this model type, a large number of distributed inelastic frame models have been proposed by several researchers [21, 28-32]. For example; Mergos and Kappos [32-33] proposed the distributed inelastic frame model using the subelement concept of Soleimani [28] and the shear-flexure interaction was triggered through the flexural deformation-dependent shear strength model. Subsequently, Zimos et al. [34] enhanced the frame model of Mergos and Kappos [32-33] with the ability to predict the onset of axial failure for non-ductile RC columns. The above-mentioned frame models could present well several intrinsic features of non-ductile RC columns, namely: the coupling effect between shear and flexure, degradation of shear resistance with increasing sectional curvature ductility, and gradual spread inelasticity. However, these models required pre-defined hysteretic moment-curvature curves and could not consider the axial-flexure interaction in a natural manner.

To remedy the aforementioned drawbacks, the fiber-section model [35] has been incorporated into nonlinear frame models to consider the axial-flexure interaction in a natural manner [36-38]. Several researchers have further enhanced the fiber-based nonlinear frame models with the ability to account for the shear-flexure interaction. For example, Marini and Spacone [39] employed equilibrium requirement at the element level to couple shear with flexural actions within the framework of the force-based Timoshenko frame formulation. Even though this frame model was very accurate and could represent the distinct features of non-ductile RC columns, the employed shear constitutive law must be calibrated on a case-by-case basis [22]. Some researchers have further elaborated the fiber-based nonlinear frame models using sophisticated multi-dimensional constitutive models to include the effects of shear-flexure interaction. For example, Ceresa et al. [40] incorporated the Modified Compression Field Theory (MCFT) proposed by Palermo and Vecchio [41] into the displacement-based Timoshenko frame model to account for shear responses at the section level. Along the same line, Mullaipudi and Ayoub [30] armed the force-based Timoshenko frame model with the ability to account for sectional shear responses using the softened membrane model (SMM) proposed by Hsu and Zhu [42]. Feng et al. [43] enhanced the displacement-based fiber frame element with the interaction between shear and flexure using the multi-axial softened damage-plasticity model [44]. Subsequently, Feng et al. [45] incorporated the multi-axial softened damage-plasticity model [44] into the force-based fiber frame element to account for the shear-flexure coupling effects. Even though these models are very accurate and able to rigorously represent the effects of shear-flexure interaction at the section level, the usage of these models has been limited among practicing structural engineers due to several constraints, namely: high implementation effort, sophisticated multi-dimensional constitutive law, high computational cost, and complicated model input parameters. A nonlinear frame model serving as a computational tool in seismic assessment procedures for existing RC frame buildings must be friendly to practicing structural engineers and adequately accurate. Such a frame model has been recently proposed by Sae-Long et al. [13] and its accuracy and performance have been assessed by correlation studies between experimental and numerical responses of non-ductile RC columns under cyclic loadings. This frame model belongs to a family of displacement-based fiber Timoshenko frame models and the shear-flexure interaction procedure modified from Mergos and Kappos [32-33] was employed to account for the adverse effects of inelastic flexural deformation on the sectional shear strength. However, computational efficiency of this frame model was limited due to inherent drawback of displacement-based finite element formulation. To reduce the gap between simplicity, accuracy, and efficiency of frame models for seismic analyses of non-ductile RC columns, the force-based finite element formulation is considered a promising choice.

Up to date, the force-based finite element formulation has gained growing interests in establishing a more efficient computational platform for inelastic analyses of structures and has been proven to be able to remedy several flaws inherent in the standard displacement-based finite element formulation [45-48]. The enhanced performance of the force-based frame model is due to the merits of employed force shape functions. These merits stem from two main observations: i) in certain structural elements, the internal force distributions along the element domain can be determined exactly, thus resulting in the "exact" finite element model; and ii) along the element domain, the internal force distributions are generally smoother than the internal deformation distributions which drastically vary across the inelastic regions (e.g. plastic hinge). Consequently, the objective of the present work is to develop a more effective frame element with shear-flexure interaction. This can be achieved by incorporating the shear-flexure interaction procedure modified from Mergos and Kappos [32-33] into the force-based finite frame formulation.

The content of the paper is presented as follows. First, a set of basic equations (strong form) of the Timoshenko frame element is introduced. Second, the virtual force principle is employed to formulate the force-based Timoshenko frame element (weak form). The classical Tonti's diagram [49] is modified and employed to conveniently present the weak form of the proposed frame element. Next, the sectional shear constitutive for non-ductile RC columns and the shear-flexure interaction procedure are presented. The modified Mergos-Kappos interaction procedure and the so-called "UCSD Shear-Strength Model" proposed by Priestley et al. [18] form the core of the shear-flexure interaction procedure adopted in the present work. Finally, capability, accuracy, and efficiency of the proposed frame element are validated through correlation studies between experimental and numerical responses of two non-ductile RC columns under cyclic loadings. The implementation of the proposed element is conducted in the general-purpose finite element platform FEAP [50].



2. A Set of Basic Equations (Strong Form)

2.1 Equilibrium

The free-body diagram of an infinitesimal part dx cut from the Timoshenko frame member is shown in Figure 1 and employed to derive the system equilibrium. Under the transverse distributed load $p_y(x)$, the axial, bending, and transverse equilibriums of this infinitesimal part yield the following relations:

$$\frac{dN_{TB}(x)}{dx} = 0 \quad (1)$$

$$\frac{dM_{TB}(x)}{dx} + V_{TB}(x) = 0 \quad (2)$$

$$\frac{dV_{TB}(x)}{dx} + p_y(x) = 0 \quad (3)$$

where $N_{TB}(x)$, $M_{TB}(x)$, and $V_{TB}(x)$ present the frame sectional axial force, bending moment, and shear force, respectively. The subscript $_{TB}$ appended to each variable denotes that the proposed element employs the Timoshenko beam theory to describe the kinematics of the frame section.

For the sake of conciseness, eqs. (1), (2), and (3) are arranged into the matrix form as:

$$\mathbf{L}_{TB}^T \mathbf{D}_{TB}(x) - \mathbf{p}(x) = \mathbf{0} \quad (4)$$

in which

$$\begin{aligned} \mathbf{D}_{TB}(x) &= \{N_{TB}(x) \quad M_{TB}(x) \quad V_{TB}(x)\}^T \\ \mathbf{p}(x) &= \{0 \quad 0 \quad p_y(x)\}^T \end{aligned} \quad (5)$$

The frame sectional force vector $\mathbf{D}_{TB}(x)$ contains the sectional axial force, bending moment, and shear force while the element distributed load vector $\mathbf{p}(x)$ contains only the transverse distributed load $p_y(x)$ in the present study. The differential operator \mathbf{L}_{TB} in eq. (4) is defined as:

$$\mathbf{L}_{TB} = \begin{bmatrix} \frac{d}{dx} & 0 & 0 \\ 0 & \frac{d}{dx} & 0 \\ 0 & 1 & -\frac{d}{dx} \end{bmatrix} \quad (6)$$

From the equilibrium requirement of eqs. (1), (2), and (3), it is clear that this system is statically determinate because there are three internal unknown forces and there are three available equilibrium equations. Therefore, the number of equilibrium equations are sufficient to compute all internal forces, and this is a key feature to derive equilibrated force shape functions.

2.2 Compatibility

The conjugate work pair of the frame sectional force vector $\mathbf{D}_{TB}(x)$ is the frame sectional deformation vector $\mathbf{d}_{TB}(x)$ which can be defined as:

$$\mathbf{d}_{TB}(x) = \{\varepsilon_{TB}(x) \quad \varphi_{TB}(x) \quad \gamma_{TB}(x)\}^T \quad (7)$$

where $\varepsilon_{TB}(x)$, $\varphi_{TB}(x)$, and $\gamma_{TB}(x)$ are, respectively, the sectional axial strain, the bending curvature, and the shear strain of the Timoshenko frame element.

Similar to the frame sectional deformation vector $\mathbf{d}_{TB}(x)$, the sectional displacement vector $\mathbf{u}(x)$ can be defined as:

$$\mathbf{u}(x) = \{u_{TB}(x) \quad \theta_{TB}(x) \quad v_{TB}(x)\}^T \quad (8)$$

where $u_{TB}(x)$, $\theta_{TB}(x)$, and $v_{TB}(x)$ represent the axial displacement at reference axis, the rotation, and the transverse displacement, respectively.

Following the kinematics assumption of the Timoshenko beam theory, the deformation-displacement relations of the frame element (compatibility condition) can be expressed as:

$$\varepsilon_{TB}(x) = \frac{du_{TB}(x)}{dx} \quad (9)$$

$$\varphi_{TB}(x) = \frac{d\theta_{TB}(x)}{dx} \quad (10)$$

$$\gamma_{TB}(x) = \theta_{TB}(x) - \frac{dv_{TB}(x)}{dx} \quad (11)$$



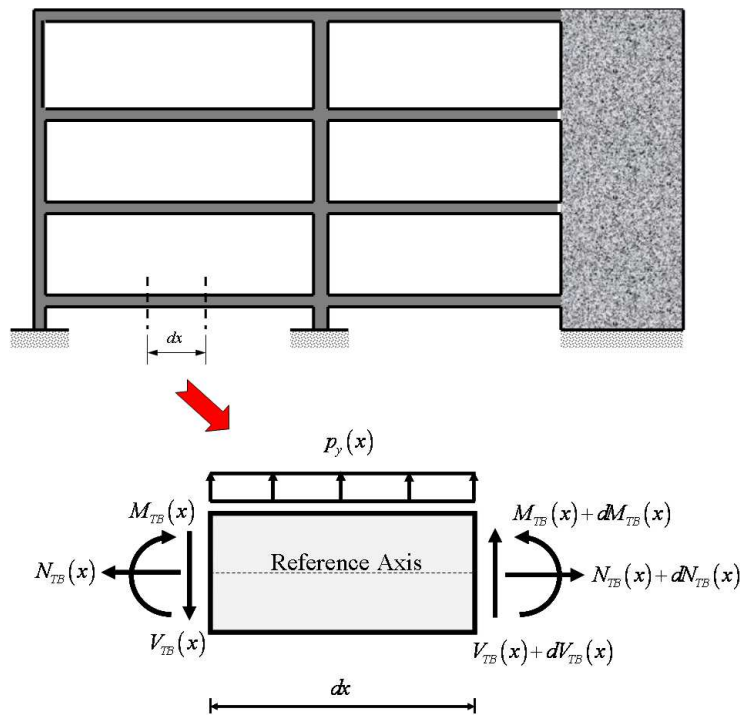


Fig. 1. Infinitesimal part dx of a frame member under transverse load $p_y(x)$.

The matrix form of eqs. (9), (10), and (11) can be written as:

$$\mathbf{d}_{TB}(x) = \mathbf{L}_{TB}\mathbf{u}(x) \tag{12}$$

It could be observed that the equilibrium equation of eq. (4) corresponds to the compatibility equation of eq. (12) via the differential operator \mathbf{L}_{TB} , thus confirming the contragradient nature between equilibrium and compatibility conditions.

2.3 Sectional Force-Deformation Relations

The relations between sectional forces and sectional deformations of an RC frame element depend on the material properties, cross-section geometries, and behaviors of the constituent materials. Generally, these nonlinear relations can be expressed in terms of the nonlinear functions $\Psi[...]$ as:

$$\mathbf{D}_{TB}(x) = \Psi[\mathbf{d}_{TB}(x)] \tag{13}$$

The force-deformation relations of eq. (13) can be expressed in a linearized incremental form as:

$$\mathbf{D}_{TB}(x) = \mathbf{D}_{TB}^0(x) + \mathbf{k}_{TB}^0(x)\Delta\mathbf{d}_{TB}(x) \tag{14}$$

where $\mathbf{D}_{TB}^0(x)$ represents the frame sectional force vector; and $\mathbf{k}_{TB}^0(x)$ is the stiffness matrix of the frame element. The superscript 0 appended on each symbol indicates the initial point of a vector or matrix during the iterative solution process.

In the present work, the fiber-section model [37] is employed to subdivide the frame cross-section into several discrete fibers (layers) as shown in Figure 2. With the fiber-section model, the axial and flexural actions are automatically coupled. Thus, the axial force $N_{TB}(x)$ and bending moment $M_{TB}(x)$ are obtained using the sectional axial-force and sectional moment equilibrium conditions as:

$$N_{TB}(x) = \sum_{n=1}^{n_{fib}} \sigma_n A_n \quad \text{and} \quad M_{TB}(x) = -\sum_{n=1}^{n_{fib}} y_n \sigma_n A_n \tag{15}$$

where σ_n , A_n and y_n are, respectively, the normal stress, the area, and the perpendicular distance from the x -axis of the n^{th} fiber in the section; n indicates the generic fiber; and n_{fib} is the number of fibers in the section.

Following the sectional axial force and bending moment expressions of eq. (15), the frame sectional force vector $\mathbf{D}_{TB}(x)$ of eq. (5) can be rewritten as:

$$\mathbf{D}_{TB}(x) = \left\{ \sum_{n=1}^{n_{fib}} \sigma_n A_n \quad -\sum_{n=1}^{n_{fib}} y_n \sigma_n A_n \quad V_{TB}(x) \right\}^T \tag{16}$$

From the frame sectional force vector $\mathbf{D}_{TB}(x)$ of eq. (16), it can be observed that the axial $N_{TB}(x)$ and flexural $M_{TB}(x)$ actions depend on the normal stress σ_n varying along the section height following the fiber-section model while the shear action $V_{TB}(x)$ is constant along the section height following the Timoshenko beam theory [51]. Thus, one-fiber discretization is sufficient to represent the sectional shear response.



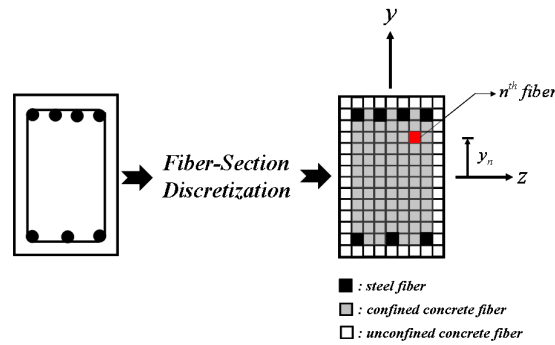


Fig. 2. Fiber-section model for RC sectional response [37].

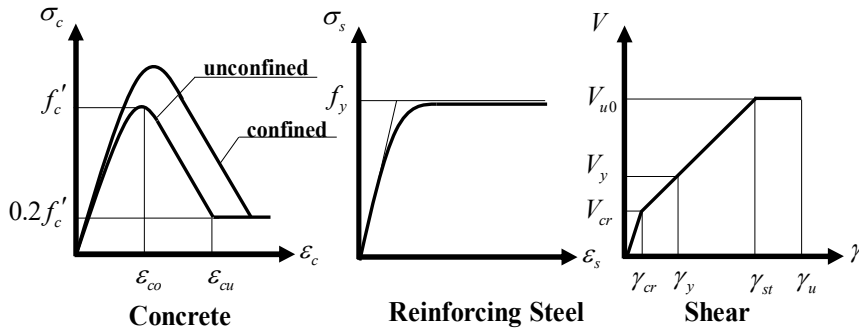


Fig. 3. Uniaxial constitutive laws for constituent materials in RC section [13].

Based on the fiber-section model, the frame sectional stiffness matrix $\mathbf{k}_{TB}(x)$ can be defined as:

$$\mathbf{k}_{TB}(x) = \begin{bmatrix} \sum_{n=1}^{n_{fib}} E_n A_n & -\sum_{n=1}^{n_{fib}} y_n E_n A_n & 0 \\ -\sum_{n=1}^{n_{fib}} y_n E_n A_n & \sum_{n=1}^{n_{fib}} y_n^2 E_n A_n & 0 \\ 0 & 0 & GA_s \end{bmatrix} \tag{17}$$

where E_n and GA_s represent the sectional modulus of the n^{th} fiber and the sectional shear stiffness, respectively. The frame sectional stiffness matrix $\mathbf{k}_{TB}(x)$ of eq. (17) demonstrates that shear action does not couple with axial and flexural actions in a direct manner. However, the shear and flexural responses are related through the adopted sectional shear strength model proposed by Priestley et al. [18] and will be discussed subsequently.

To describe the nonlinear response of an RC frame section, this study uses three uniaxial cyclic constitutive laws, namely: Kent and Park model [52] for concrete; Menegotto and Pinto model [53] for reinforcing steel bars; and modified Mergos and Kappos model [13] for sectional shear response. Primary response curves of each constitutive model are shown in Figure 3.

As required in the force-based finite element formulation, the frame sectional flexibility matrix $\mathbf{f}_{TB}(x)$ can be obtained from consistent inverse of the frame sectional stiffness matrix $\mathbf{k}_{TB}(x)$, thus resulting in the following expression:

$$\mathbf{d}_{TB}(x) = \mathbf{d}_{TB}^0(x) + \mathbf{f}_{TB}(x) \Delta \mathbf{D}_{TB}(x) \tag{18}$$

3. Force-Based Finite Frame Formulation

3.1 Formulation

The present work adopts the general framework of the force-based frame element formulation and its implementation procedure originally proposed by Spacone et al. [36] and subsequently modified by Limkatanyu and Spacone [46]. In this type of finite element formulation, the sectional forces $\mathbf{D}_{TB}(x)$ serving as primary variables are determined directly from the element nodal forces through equilibrated force shape functions. Consequently, the element equilibrium requirement of eq. (4) is satisfied in a point-wise sense. The element compatibility requirement of eq. (12) is expressed through the weighted residual statement. As a result, the element compatibility requirement is enforced in an integral sense. The summarized framework of the proposed force-based frame element formulation is presented in the modified Tonti's diagram of Figure 4 [49].

The compatibility condition of eq. (12) is written in the weighted residual form as:

$$\int_L \delta \mathbf{D}_{TB}^T(x) [\mathbf{d}_{TB}(x) - \mathbf{L}_{TB} \mathbf{u}(x)] dx = 0 \tag{19}$$

where $\delta \mathbf{D}_{TB}(x)$ is the statically admissible virtual section force vector. Substituting the linearized deformation-force relations of eq. (18) into eq. (19) leads to:



$$\int_L \delta \mathbf{D}_{TB}^T(x) [\mathbf{d}_{TB}^0(x) + \mathbf{f}_{TB}^0(x) \Delta \mathbf{D}_{TB}(x) - \mathbf{L}_{TB} \mathbf{u}(x)] dx = 0 \tag{20}$$

In order to move the differential operator \mathbf{L}_{TB} from the displacement vector $\mathbf{u}(x)$ to the virtual force vector $\delta \mathbf{D}_{TB}(x)$, integration by parts is applied to eq. (20), leading to the following expression:

$$\begin{aligned} & \int_L \delta \mathbf{D}_{TB}^T(x) \mathbf{f}_{TB}^0(x) \Delta \mathbf{D}_{TB}(x) dx + \int_L \delta \mathbf{D}_{TB}^T(x) \mathbf{d}_{TB}^0(x) dx \\ &= \delta \bar{\mathbf{P}}^T \bar{\mathbf{U}} + \int_L \mathbf{u}(x) \left[\frac{\mathbf{L}_{TB}^T \delta \mathbf{D}_{TB}(x)}{\delta \mathbf{p}(x)} \right] dx \end{aligned} \tag{21}$$

where the scalar-product term $\delta \bar{\mathbf{P}}^T \bar{\mathbf{U}}$ resulting from the integration by parts represents the end-boundary complementary virtual work done by the virtual basic nodal forces $\delta \bar{\mathbf{P}}$ on the basic nodal displacements $\bar{\mathbf{U}}$. Clearly, eq. (21) defines the complementary virtual work expression of the system. The terms on the left-hand side of eq. (21) represent the complementary internal virtual work δW_{int}^* while the terms on the right-hand side represent the complementary external virtual work δW_{ext}^* . Recalling the equilibrium condition of eq. (4) and arbitrarily selecting the virtual element distributed load vector $\delta \mathbf{p}(x) = \mathbf{0}$, eq. (21) becomes:

$$\int_L \delta \mathbf{D}_{TB}(x)^T \mathbf{f}_{TB}^0(x) \Delta \mathbf{D}_{TB}(x) dx = \delta \bar{\mathbf{P}}^T \bar{\mathbf{U}} - \int_L \delta \mathbf{D}_{TB}(x)^T \mathbf{d}_{TB}^0(x) dx \tag{22}$$

eq. (22) represents the core expression of the proposed force-based frame formulation and will be subsequently discretized to obtain the finite element equation. The discrete form of eq. (22) can be obtained by expressing the sectional forces $\mathbf{D}_{TB}(x)$ in terms of the element nodal forces without rigid-body modes (basic element nodal forces) $\bar{\mathbf{P}}$ using equilibrated force shape functions. The interpolation relation between the sectional forces $\mathbf{D}_{TB}(x)$ and the basic element nodal forces $\bar{\mathbf{P}}$ can thus be written as:

$$\mathbf{D}_{TB}(x) = \mathbf{N}_{TB}^{F-B}(x) \bar{\mathbf{P}} \tag{23}$$

where the matrix $\mathbf{N}_{TB}^{F-B}(x)$ contains equilibrated force shape functions. The superscript $F-B$ emphasizes the force-based finite frame formulation. For the adopted simply-supported system shown in Figure 5, the force-shape function matrix $\mathbf{N}_{TB}^{F-B}(x)$ is:

$$\mathbf{N}_{TB}^{F-B}(x) = \begin{bmatrix} N_{TB1}^{F-B}(x) & 0 & 0 \\ 0 & N_{TB2}^{F-B}(x) & N_{TB3}^{F-B}(x) \\ 0 & -\frac{dN_{TB2}^{F-B}(x)}{dx} & -\frac{dN_{TB3}^{F-B}(x)}{dx} \end{bmatrix} = \begin{bmatrix} 1 & 0 & 0 \\ 0 & \frac{x}{L} - 1 & \frac{x}{L} \\ 0 & -\frac{1}{L} & -\frac{1}{L} \end{bmatrix} \tag{24}$$

It is worth emphasizing that with these force shape functions, the equilibrium condition of eq. (4) is enforced in a point-wise manner. The element flexibility equation can be gained by substituting eq. (23) into eq. (22) and subsequently accounting for the arbitrariness of $\delta \bar{\mathbf{P}}$, thus resulting in:

$$\mathbf{F}_{TB}^0(x) \Delta \bar{\mathbf{P}} = \bar{\mathbf{U}} - \bar{\mathbf{U}}_r^0 \tag{25}$$

where $\mathbf{F}_{TB}^0(x) = \int_L (\mathbf{N}_{TB}^{F-B}(x))^T \mathbf{f}_{TB}^0(x) \mathbf{N}_{TB}^{F-B}(x) dx$ represents the element flexibility matrix.

The element nodal displacements $\bar{\mathbf{U}}_r^0$ in eq. (25) are weakly compatible with the frame section deformations $\mathbf{d}_{TB}^0(x)$ through the following integral expression:

$$\bar{\mathbf{U}}_r^0 = \int_L (\mathbf{N}_{TB}^{F-B}(x))^T \mathbf{d}_{TB}^0(x) dx \tag{26}$$

It is worthwhile to remark that the term $\bar{\mathbf{U}} - \bar{\mathbf{U}}_r^0$ on the right-hand side of eq. (25) represents the residual element nodal displacements and corresponds to the integral statement of compatibility condition of eq. (12). During the incremental-iterative solution process, this residual vector will vanish once the element section deformations are compatible with the element nodal displacements.

In the present study, the general-purpose finite element platform FEAP [50] is employed to host the proposed frame element. The platform architect of FEAP is constructed within the framework of stiffness-based finite element formulation, thus rendering FEAP natural to the stiffness-based finite element model. To implement the proposed force-based frame element into the platform of displacement-based finite element software, rigid body modes must be injected and filtered out during the element state determination process. Thus, the rigid-body-mode transformation matrix \mathbf{T}_{RBM} is required between the systems with and without rigid body modes. This study adopts the simply-supported system to eliminate the rigid body motions as shown in Figure 6. The transformation relations between the element nodal forces, element nodal displacements, and element stiffness matrices with respect to systems with and without rigid-body modes are given as:

$$\begin{aligned} \mathbf{P} &= \mathbf{T}_{RBM}^T \bar{\mathbf{P}} \\ \bar{\mathbf{U}} &= \mathbf{T}_{RBM} \mathbf{U} \\ \mathbf{K} &= \mathbf{T}_{RBM}^T \bar{\mathbf{K}} \mathbf{T}_{RBM} \end{aligned} \tag{27}$$



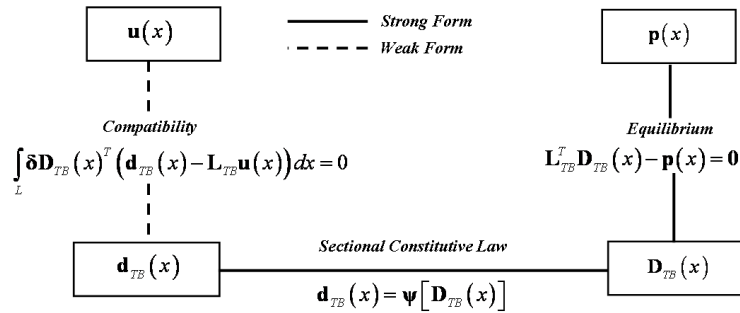


Fig. 4. Modified Tonti's diagram for RC frame element: Force-based formulation (Weak form).

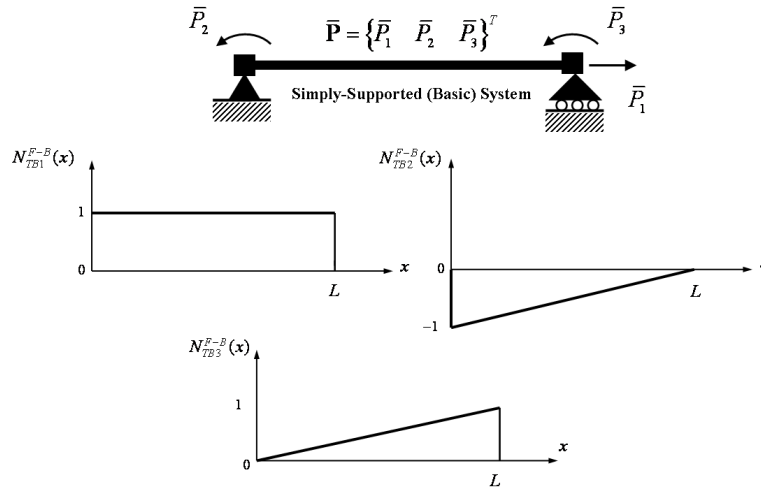


Fig. 5. Equilibrated force shape functions associated with simply-supported (basic) system.

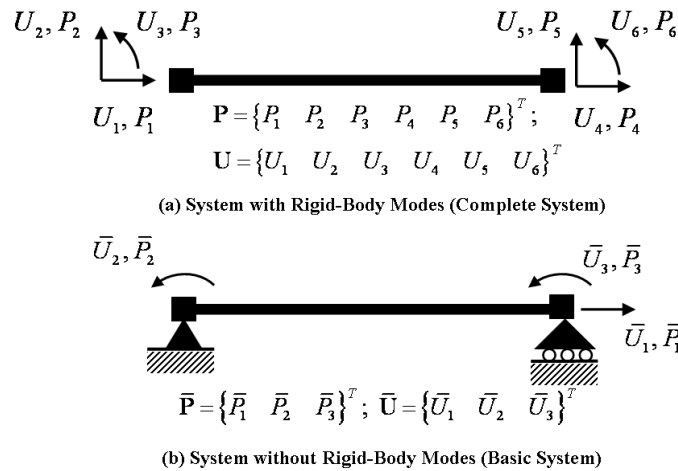


Fig. 6. Element force and displacement degrees of freedom: (a) Complete system; and (b) Basic system.

In addition to the transformation relations of eq. (27), a special procedure for the element state determination is required for the proposed frame element formulated within the framework of flexibility-based finite element model. The state-of-the-art procedure for implementing the flexibility-based finite element model into the stiffness-based computational platform was proposed by Spacone et al. [54] and Limkatanyu and Spacone [55]. This procedure is adopted in the present work and is briefly discussed herein.

For a given current nodal displacement increment, the current nodal force increment is computed using the initial (previous iterative step) element stiffness matrix and is used to update the nodal force vector. Then, the current section force increment associated with the current nodal force increment is computed using the force shape functions and the section force vector is updated accordingly. Next, the current section deformation increment associated with the current section force increment is computed using the initial (previous iterative step) section flexibility matrix and the section deformation vector is updated accordingly. With the updated current section deformation vector, the associated section force vector and the associated section stiffness (flexibility) matrix can be obtained via the section constitutive relations. Generally, the current section force vector obtained from the section constitutive relations is not in equilibrium with the current nodal force vector, thus resulting in an unbalanced section force vector and the associated residual section deformation vector. The residual nodal displacement vector is computed from the residual section deformation vector using the integral expression of element compatibility. Finally, the unbalanced nodal force vector is computed from the residual nodal displacement vector and is passed from the element level to the structural level during the incremental-iterative solution process. More details on the above-discussed element state determination procedure can be found in Spacone et al. [54] and Limkatanyu and Spacone [55].



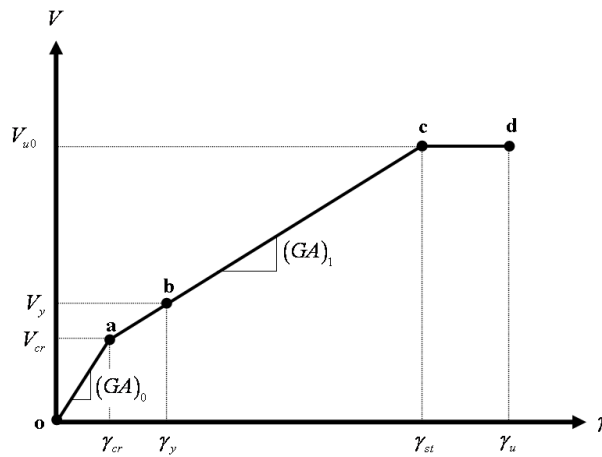


Fig. 7. Undamaged (primary) envelope curve for sectional shear response [13].

4. Sectional Shear Constitutive Law

4.1 Undamaged Primary Curve

The relation between the sectional shear force and shear strain in the present work stems from the undamaged primary curve shown in Figure 7. Originally, this curve was presented by Mergos and Kappos [32-33] and later modified by Zimos et al. [34] and Sae-Long et al. [13].

On the curve, there are four parts with three different slopes. The first part with a linear portion *oa* and slope $(GA)_0$ shows the uncracked behavior of reinforced concrete and connects the origin point *o* to the point *a* (V_{cr}, γ_{cr}) at which the sectional concrete starts cracking. The point *a* is associated with the stress state at which the nominal principal tensile stress reaches the nominal tensile strength of concrete. To compute the cracking shear force V_{cr} , the uncracked shear slope $(GA)_0$, and the cracking shear strain γ_{cr} , Sezen and Moehle [19] proposed the following expression:

$$\begin{aligned}
 V_{cr} &= \left(\frac{f'_t}{(L_a/h)} \sqrt{1 + \frac{N}{f'_t A_g}} \right) 0.80 A_g \\
 (GA)_0 &= 0.80 GA_g \\
 \gamma_{cr} &= \frac{V_{cr}}{(GA)_0}
 \end{aligned}
 \tag{28}$$

where f'_t is the nominal tensile concrete strength; L_a/h is the shear span ratio; A_g is the gross cross sectional area; and G is the concrete shear modulus.

The second part with a linear portion *ab* and slope $(GA)_1$ represents the sectional shear response between the cracking point *a* (V_{cr}, γ_{cr}) and the first plastic-hinge formation point *b* (V_y, γ_y). The point *b* is associated with the state at which the longitudinal reinforcement experiences yielding for the first time. This point is detected with the fiber-section model.

The third part with a linear portion *bc* has the same slope as the second part $(GA)_1$ and represents the sectional shear response after the plastic hinge is triggered. This part links the flexural-yielding point *b* (V_y, γ_y) to the point *c* (V_{u0}, γ_{st}) at which the sectional shear force attains its ultimate value V_{u0} while the shear strain reaches the value at the onset of transverse reinforcement yielding γ_{st} . To determine the sectional shear strength, this study employs the so-called “UCSD Shear-Strength Model” proposed by Priestley et al. [18]. The UCSD shear strength V_{u0} is:

$$V_{u0} = k_\varphi \sqrt{f'_c} (0.8 A_g) + \frac{A_v f_{yv} D'}{s} \cot 30^\circ + N \tan \beta
 \tag{29}$$

where f'_c is the concrete compressive strength; k_φ is a reduction factor for the concrete shear-strength contribution and is a function of the flexural curvature ductility μ_φ as shown in Figure 8; s is the spacing of transverse reinforcement; A_v is the cross-section area of the transverse reinforcement; f_{yv} is the yield strength of the transverse reinforcement; N is the member axial force; D' is the distance measured parallel to the applied shear between centers of the longitudinal reinforcement; and β is the angle between the member axis and the line connecting the centers of the flexural compression zones at the top and the bottom of the column ends.

The shear strain at the onset of transverse reinforcement yielding γ_{st} can be determined using the truss analogy approach [56]. However, the resulting value of shear strain γ_{st} did not coincide well with values obtained from experimental results. Subsequently, Mergos and Kappos [32-33] enhanced this approach with two modification factors based on regression analysis. The first factor κ considers the axial-load effect while the second factor λ accounts for the member-aspect ratio effect. The shear strain γ_{st} is thus modified as:

$$\gamma_{st} = \kappa \lambda \gamma_{truss}
 \tag{30}$$



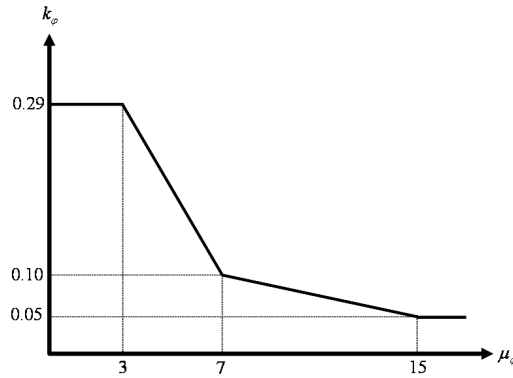


Fig. 8. Relationship between imposed curvature ductility μ_ϕ and concrete shear strength reduction factor contribution k_ϕ [32].

where $\kappa = 1 - 1.07(N / f'_c A_g)$ is the axial-force modification factor; $\lambda = 5.37 - 1.59 \min(2.5, L_a / h)$ is the modification factor associated the member-aspect-ratio; and γ_{truss} represents the shear strain corresponding to the transverse reinforcement yielding as computed from the truss analogy approach [56] and is defined in eq. (31) as:

$$\gamma_{truss} = \frac{V_{cr}}{(GA)_0} + \frac{A_w f_{yv}}{s E_s b \rho_w \sin^4 \psi \cot \psi} \left(\sin^4 \psi + \frac{E_s}{E_c} \rho_w \right) \tag{31}$$

where E_s and E_c define respectively the elastic moduli for steel and concrete; b is the sectional width; ρ_w represents the volumetric ratio of the transverse reinforcement; and ψ is the angle between the member reference axis and the line of diagonal struts. The optimal value of angle $\psi = 45^\circ$ in this study follows the research work by Mergos and Kappos [32].

Finally, the last part with a flat-top linear portion cd presents the plastic sectional shear response. This part connects the shear-yielding point $c (V_{u0}, \gamma_{st})$ to the ultimate point $d (V_{u0}, \gamma_u)$ at which the shear strain attains its ultimate value γ_u . This part of the sectional shear response is in compliance with experimental evidences that the shear strain of shear-critical and flexure-shear critical RC columns could further increase even after yielding of transverse reinforcement until they reach the failure state [14-17, 32, 57-60]. Thus, the value of the shear strain γ_u could be larger than the value of the yielding shear strain γ_{st} . Based on regression analyses of 25 RC shear-critical and flexure-shear critical columns, Mergos and Kappos [32] suggested the following expression for γ_u :

$$\gamma_u = \lambda_1 \lambda_2 \lambda_3 \gamma_{st} \geq \gamma_{st} \tag{32}$$

The ultimate shear strain γ_u is computed based on the yielding shear strain γ_{st} using three modification factors, namely: $\lambda_1 = 1 - 2.5 \min(0.4, N / f'_c A_g)$ accounting for the axial-load effect; $\lambda_2 = \min(6.25, L_a^2 / h^2)$ considering the member aspect ratio; and $\lambda_3 = 0.31 + 17.8 \min(A_w f_{yv} / bs f'_c, 0.08)$ taking into account the amount of transverse reinforcement.

4.2 Modified Mergos-Kappos Shear-Flexural Interaction Procedure

The strong coupling between shear and flexural actions in RC columns has long been noticed in the structural engineering research community. Several research work has been conducted both experimentally and analytically to demonstrate the detrimental effect of inelastic flexural deformations on the sectional shear capacity [15-18, 32, 33, 61]. This shear-flexure interaction is particularly critical in characterizing the response of non-ductile RC columns.

In the present work, the so-called “modified Mergos-Kappos” shear-flexure interaction procedure is adopted and incorporated into the proposed force-based frame model. This shear-flexure interaction procedure originally proposed by Mergos and Kappos [32-33] was modified and employed by Sae-Long et al. [13] with success to account for the shear-flexure interaction effect for non-ductile RC columns. For the sake of self-containment, general description of the modified Mergos-Kappos shear-flexure interaction procedure is repeated herein.

Figure 9 presents a big picture of the modified Mergos-Kappos shear-flexure interaction procedure and the evolution of the reduced shear envelope curve with increasing curvature ductility μ_ϕ . As dictated in the UCSD shear-strength model [18], reduction in the sectional shear strength is associated with degradation of the concrete shear-strength component $V_c = k_\phi \sqrt{f'_c} (0.8 A_g)$ appearing in eq. (29). The sectional shear response starts to deviate from the undamaged envelope curve once the shear strength degradation is triggered. The damaged (reduced) envelope curve is kept updating with the evolution of the degraded shear strength and the resulting envelope curve is along the response path $o - a - b - e - f' - g' - h' - c^g - d^g$.

For a given incremental sectional shear strain $\Delta\gamma$, the sectional shear state determination process computes the shear force increment ΔV and the effective sectional shear stiffness $(GA)_{eff}$. In the modified Mergos-Kappos shear-flexure interaction procedure [13], the reference shear stiffness $(GA_{ref})_i^k$ is proposed and defined as:

$$(GA_{ref})_i^k = \frac{V_{0,i}^{k+1} - V^k}{\Delta\gamma_i^k} \tag{33}$$



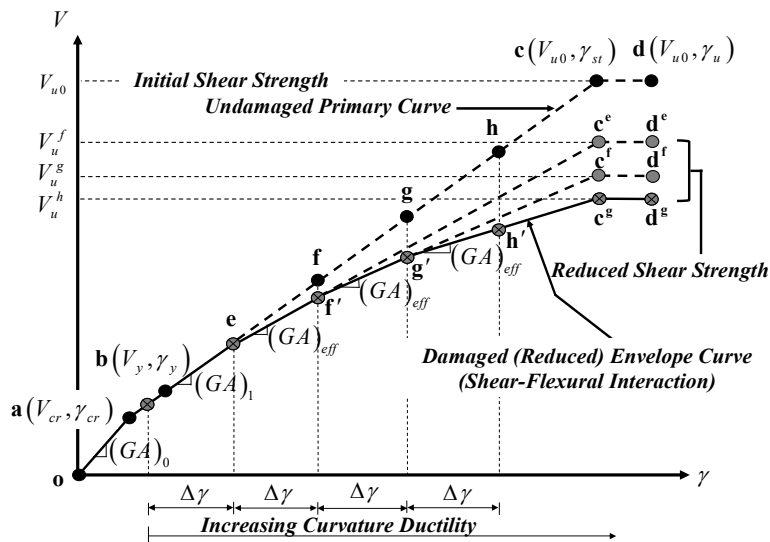


Fig. 9. Schematic representation of modified Mergos-Kappos shear-flexure interaction procedure [13].

where $V_{0,i}^{k+1} = V_{cr} + (GA)_i(\gamma_i^{k+1} - \gamma_{cr})$ represents the sectional shear force with no degradation associated with the increasing curvature ductility demand; and $\gamma_i^{k+1} = \gamma^k + \Delta\gamma_i^k$ is the current shear strain.

Considering the geometric relation between the sectional shear strain increment $\Delta\gamma_i^k$ and the sectional shear force increment ΔV_i^k leads to the following expression:

$$\Delta\gamma_i^k = \frac{\Delta V_i^k}{(GA_{eff})_i^k} = \frac{\Delta V_i^k + (\Delta V_c^{deg})_i^k}{(GA_{ref})_i^k} \tag{34}$$

where $(\Delta V_c^{deg})_i^k$ is the degraded part of the shear force corresponding to the concrete shear strength degradation and can be expressed as:

$$(\Delta V_c^{deg})_i^k = (GA_{ref})_i^k \Delta\gamma_i^k - \left(\frac{V_{ui}^k - V^k}{\gamma_{st}^k - \gamma^k} \right) \Delta\gamma_i^k \tag{35}$$

where V_{ui}^k is the curvature ductility-dependent shear strength and is a function of a reduction factor k_φ .

Solving eq. (34) for the effective sectional shear stiffness $(GA_{eff})_i^k$ leads to the following expression:

$$(GA_{eff})_i^k = \frac{\Delta V_i^k}{\Delta V_i^k + (\Delta V_c^{deg})_i^k} (GA_{ref})_i^k \tag{36}$$

It is noticed in eq. (36) that the effective sectional shear stiffness $(GA_{eff})_i^k$ and the sectional shear force increment ΔV_i^k are unknown and mutually dependent. Therefore, an additional iterative procedure is required within the element iterative step i of the load increment k and an iterative index “j” is appended to variables $(GA_{eff})_i^k$ and ΔV_i^k . It is worth remarking that the following variables $(GA_{ref})_i^k$, $(\Delta V_c^{deg})_i^k$, and $\Delta\gamma_i^k$ do not vary during this additional iterative process. The step-by-step algorithm to determine the effective sectional shear stiffness $(GA_{eff})_{i,j}^k$ and the current sectional shear force V_i^{k+1} within the modified Mergos-Kappos shear-flexure interaction procedure is shown in Figure 10. More details of the modified Mergos-Kappos shear-flexure interaction procedure can be found in Sae-Long et al. [13].

4.3 Hysteretic Law of the Sectional Shear Response

In the present study, hysteretic law of the sectional shear constitutive model follows the one presented in Sae-Long et al. [13]. This adopted hysteretic law is modified from the general hysteretic model proposed by Filippou et al. [62] and later modified by Martino [63]. Generally, this hysteretic shear model is very attractive since it represents well the pinching effect and damage corresponding to the shear resisting mechanism. The general feature of the adopted shear hysteretic model is shown in Figure 11 and its brief description is worth repeating herein for the sake of self-containment.

In Figure 11, the shear response starts from the unloaded state at point O. Then, the section is loaded along the monotonic branch O-A-B until it reaches the unloading state along the branch B-C with the uncracked stiffness $(GA)_0$. This unloading state continues until it touches the abscissa axis at point C. Then, the reloading state is triggered along the branch C-D-E in the opposite direction. During the reloading branch C-D-E, the section encounters the crack closing process before it connects to the monotonic envelope branch D-E. Unloading state takes place at point E with the uncracked stiffness $(GA)_0$ and continues until it touches the abscissa axis at point F. Then, the reloading state starts from point F along the branch F-G-H in the opposite direction. The section experiences the crack closing process, thus resulting in the pinching response along the reloading branch F-G-H. Finally, the branch H-I-J continues to the failure point J. More details on the adopted shear hysteresis model can be found in Martino [63] and Sae-Long et al. [13].



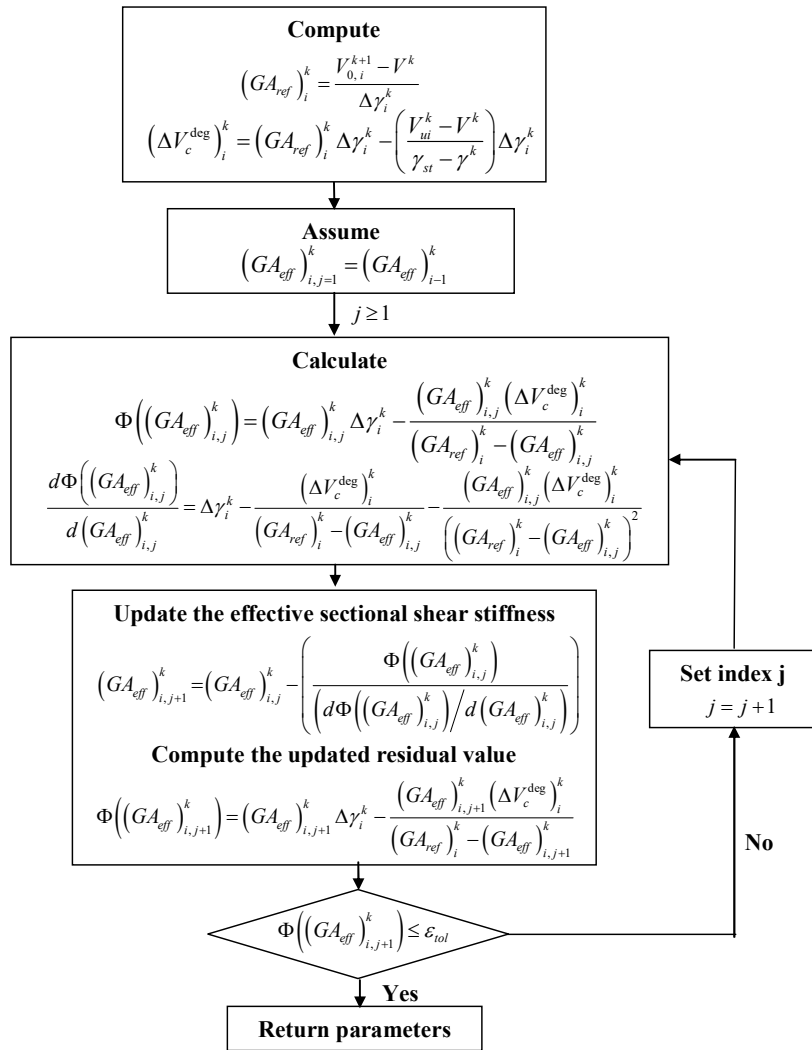


Fig. 10. Iterative algorithm for calculating effective sectional shear stiffness $(GA_{eff})_i^k$ based on modified Mergos-Kappos shear-flexure interaction procedure [13].

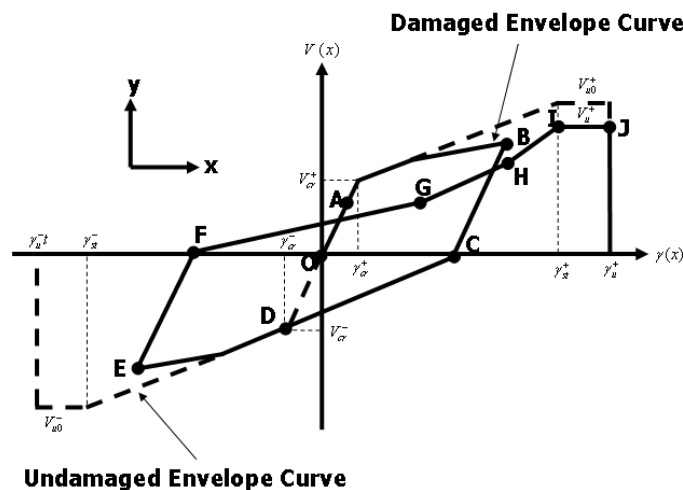
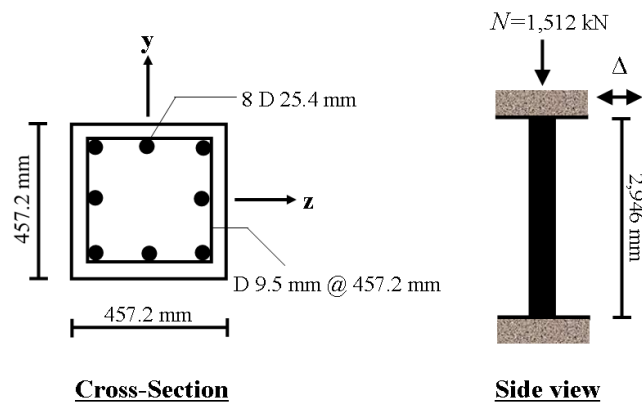


Fig. 11. Cyclic behavior of sectional shear force-shear strain response.

5. Model Validation

To verify performance and accuracy of the proposed frame element and to investigate influences of the coupling effect between shear and flexure on both global and local responses, correlation studies on two non-ductile RC columns under cyclic loadings are carried out. Both columns are considered as flexure-shear critical members, which eventually fail in shear after experiencing flexural yielding. For each proposed frame element, the element cross-section is discretized into forty fibers (layers) to obtain the sectional force-deformation response and five Gauss-Lobatto integration points are used for the element numerical integration.





Concrete: $f'_c = 25.5$ MPa
 Longitudinal reinforcement: $f_{yt} = 331$ MPa
 Transverse reinforcement: $f_{yv} = 400$ MPa

Fig. 12. Column specimen 2CMH18 [7].

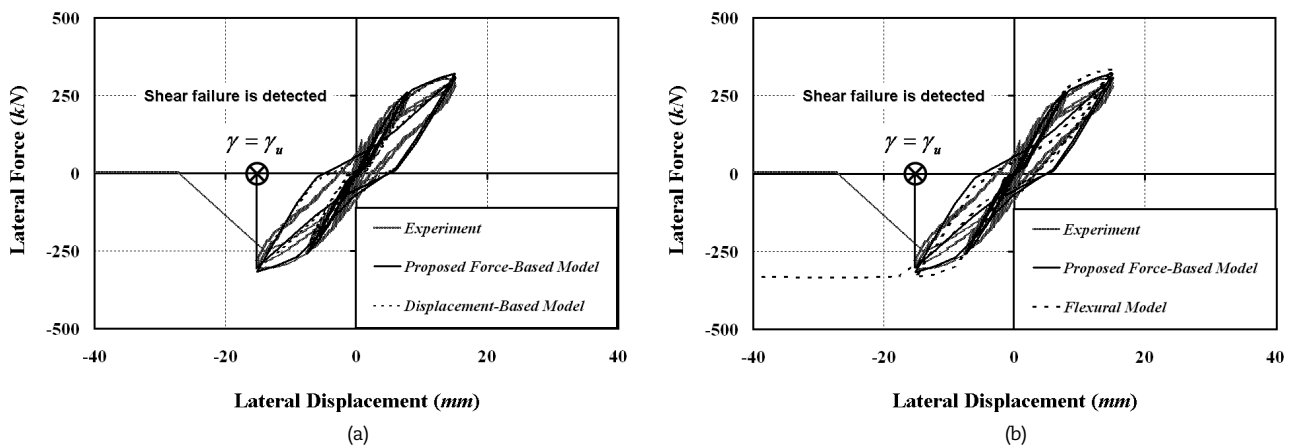


Fig. 13. Experimental and numerical responses of column specimen 2CMH18: (a) Shear-flexure interaction models; and (b) Flexural model.

5.1 Column 2CMH18

Lynn [7] tested a group of square cross-section RC columns subjected to reversed lateral displacements and a constant axial load. Details and amounts of column longitudinal and transverse reinforcement are intended to represent columns constructed before the 1970's. Therefore, these column specimens were considered as columns with seismically-substandard reinforcing details.

In the present study, one of these column specimens, column 2CMH18, is selected to examine the performance and accuracy of the proposed element and to demonstrate the essence of considering the shear-flexure interaction effect. The material properties, reinforcement details, and geometry of this column specimen are shown in Figure 12.

Figure 13 compares the experimental lateral load-displacement response with numerical lateral load-displacement responses obtained with three frame models, namely: i) the proposed force-based frame model; ii) the displacement-based frame model by Sae-Long et al. [13]; and iii) the flexural frame model by Spacone et al. [36]. In Figure 13 (a), only four proposed force-based frame elements are sufficient to resemble the salient characteristics of the experimental force-displacement response including the general shape of hysteretic response, the amount of dissipated hysteretic energy, and the member capacity. It is noted that column 2CMH18 was employed to validate the displacement-based frame model proposed by Sae-Long et al. [13]. To satisfactorily resemble the force-displacement response of this column, sixteen displacement-based frame elements of Sae-Long et al. [13] were required as shown in Figure 13 (a), thus confirming the superiority of the proposed force-based frame model over the displacement-based frame model. The lateral displacement Δ_y^{F-B} and the sectional shear strain γ_y^{F-B} associated with the plastic-hinge formation are $\Delta_y^{F-B} = 8.13$ mm and $\gamma_y^{F-B} = 1.13 \times 10^{-3}$ as predicted by the proposed force-based frame model. These values correspond well with those predicted by sixteen displacement-based frame elements of Sae-Long et al. [13]; namely: $\Delta_y^{D-B} = 8.30$ mm and $\gamma_y^{D-B} = 1.21 \times 10^{-3}$. The ultimate lateral displacement $\Delta_u^{F-B} = 15.21$ mm associated with the ultimate shear strain γ_u is predicted by the proposed force-based frame model and complies well with that obtained from experiment ($\Delta_u^{Exp} = 15.30$ mm). To emphasize the essence of shear-flexure interaction effect on characterization of non-ductile RC columns, the flexural frame model by Spacone et al. [36] is also employed to analyze column 2CMH18 and the resulting numerical response is shown in Figure 13 (b). Even though the flexural frame model can represent well the general shape of hysteretic response, the amount of dissipated hysteretic energy and the member capacity, the "flexure-shear" critical feature inherent to column 2CMH18 cannot be accounted for.



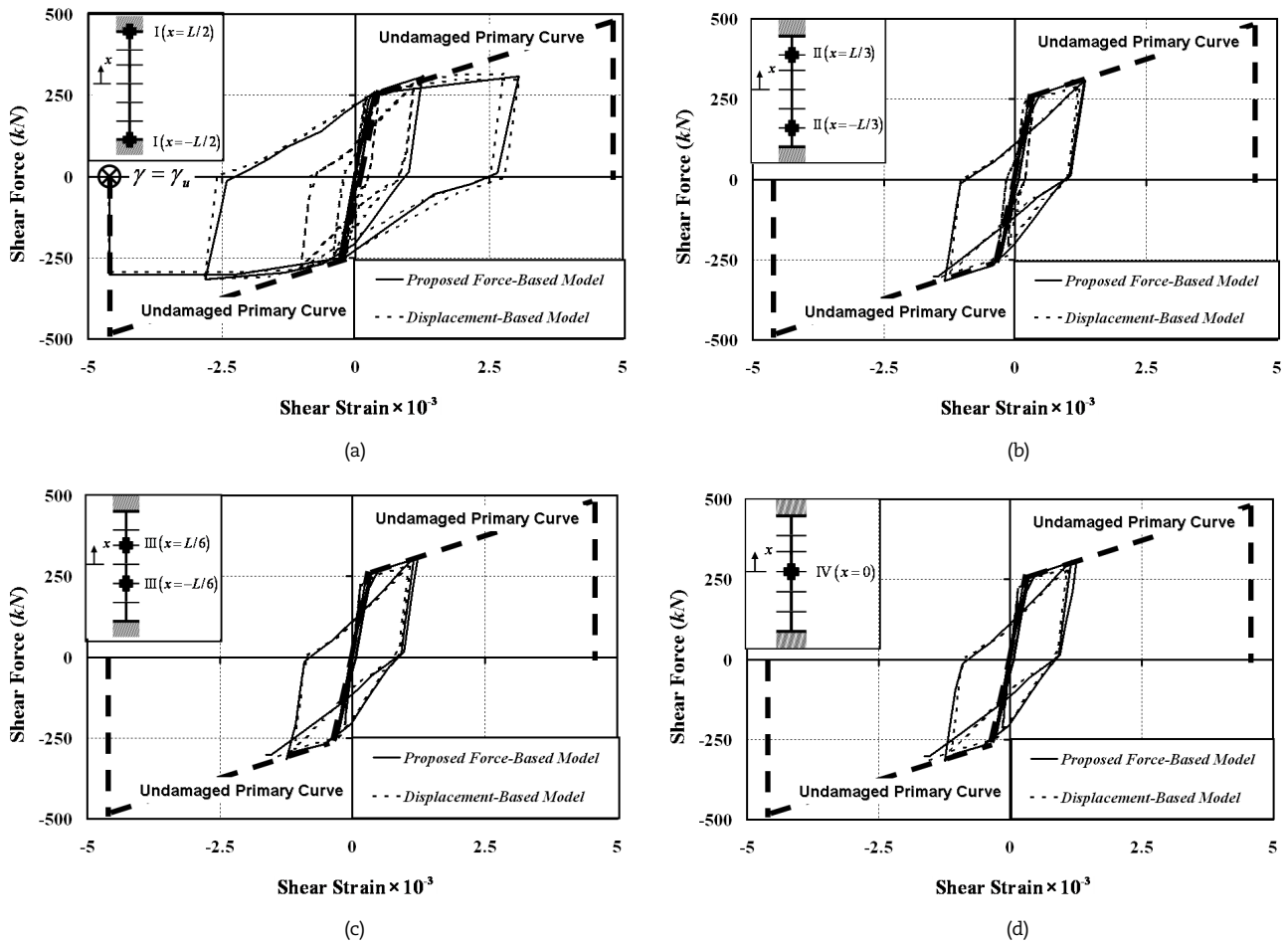


Fig. 14. Sectional shear responses along column specimen 2CMH18: Proposed force-based model vs. displacement-based model.

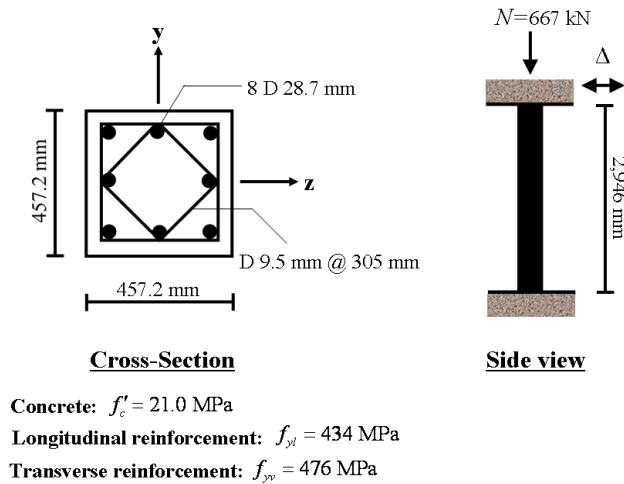


Fig. 15. Column specimen 2CLD12 [15].

Figure 14 presents the hysteretic shear responses at various positions along the column height (Section I, II, III, and IV) obtained with the proposed force-based frame model, together with those obtained with sixteen displacement-based frame elements by Sae-Long et al. [13]. Comparison between the two frame models confirms accuracy of the proposed force-based frame model in representing the local (sectional) responses. It is observed that the shear response in Section I locating inside the plastic-hinge region drastically differs from those at all other section positions resting outside the plastic-hinge region due to the shear-flexure interaction. As shown in Figure 14 (a), the sectional shear response at Section I starts to deviate from the undamaged envelope curve when the sectional curvature ductility μ_ϕ reaches its threshold value of 3 as governed by the UCSD shear-strength model. On the other hand, Section II, III and IV (respectively in Figure 14 (b), (c) and (d)) response cyclically with respect to the undamaged envelope curve and behave almost identically. This observation stems from the fact that shear-flexure interaction is not triggered at those sections since they are outside the plastic-hinge zone.



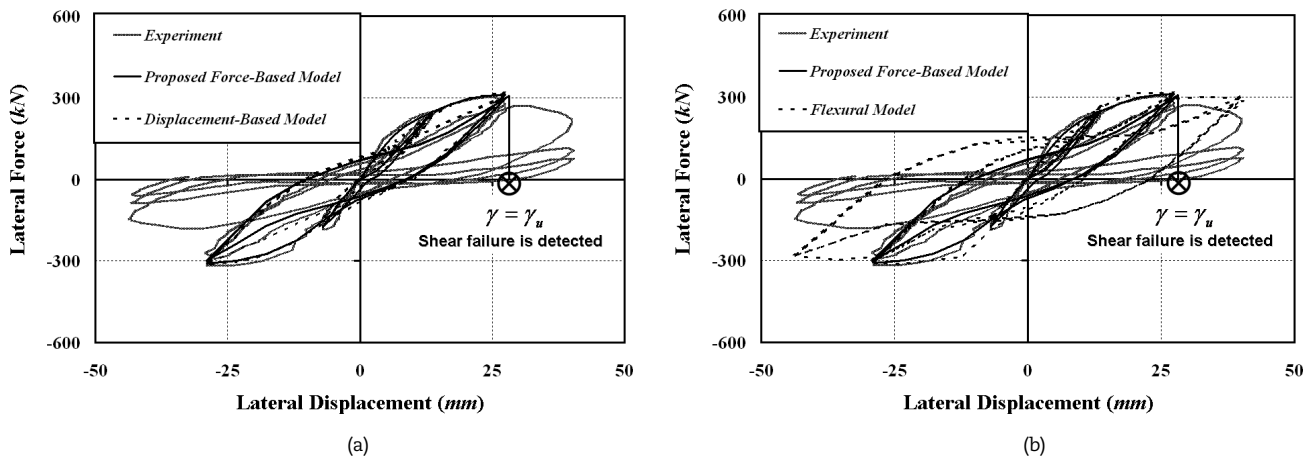


Fig. 16. Experimental and numerical responses of column specimen 2CLD12: (a) Shear-flexure interaction models; and (b) Flexural model.

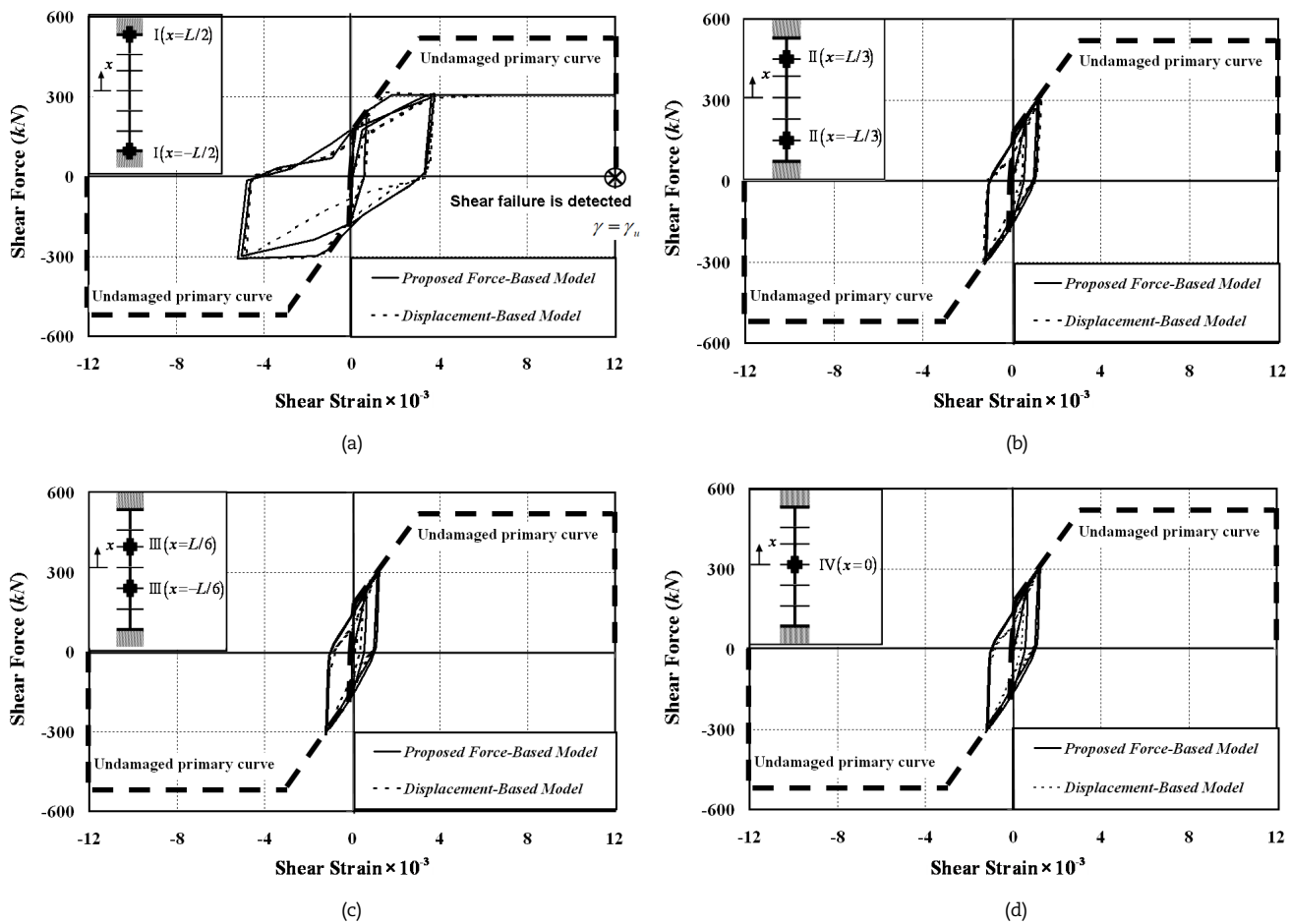


Fig. 17. Sectional shear responses along column specimen 2CLD12: Proposed force-based model vs. displacement-based model.

5.2 Column 2CLD12

Sezen [15] tested a set of four full-scale columns representing existing columns with insufficient transverse reinforcement and poor seismic resistance details. These columns were tested in double bending action under cyclic lateral displacements and subjected to a constant axial load. One of the column specimens labeled column 2CLD12 is selected here to validate the proposed force-based frame element and to demonstrate the influence of inelastic bending deformations on sectional shear response. Mergos and Kappos [33] and Sae-Long et al. [13] also employed this column specimen to verify their frame elements with inclusion of shear-flexure interaction. Material properties, reinforcement details, and dimensions of this column provided by Sezen [15] are shown in Figure 15.

Figure 16 compares the experimental lateral load-displacement responses with numerical lateral load-displacement responses obtained with three frame models, namely: i) the proposed force-based frame model; ii) the displacement-based frame model by Sae-Long et al. [13]; and iii) the flexural frame model by Spacone et al. [36]. Figure 16 (a) indicates that only four proposed force-based frame elements can present well several features of the experimental result. These features are the initial



stiffness, the general shape of the hysteretic response, the member capacity, and the amount of dissipated hysteretic energy. To obtain the same level of accuracy, sixteen displacement-based frame elements by Sae-Long et al. [13] were, thus emphasizing superiority of the proposed force-based frame model over the displacement-based frame model. As predicted by the proposed force-based frame model, the lateral displacement Δ_y^{F-B} and the sectional shear strain γ_y^{F-B} associated with plastic-hinge formation are $\Delta_y^{F-B} = 13.3$ mm and $\gamma_y^{F-B} = 1.45 \times 10^{-3}$, respectively. These predicted values are in close agreement with those predicted by the displacement-based frame model of Sae-Long et al. [13]; namely: $\Delta_y^{D-B} = 13.8$ mm and $\gamma_y^{D-B} = 1.58 \times 10^{-3}$. The ultimate lateral displacement $\Delta_u^{F-B} = 28.15$ mm associated with the ultimate shear strain γ_u is predicted by the proposed force-based frame model and is in good agreement with that obtained from experiment ($\Delta_u^{Exp} = 28.0$ mm).

To bring out necessity of the shear-flexure coupling effect in predicting the column failure mode, column 2CMH18 is also analyzed by the flexural frame model of Spacone et al. [36] and the resulting numerical response is plotted in Figure 16 (b). Generally, the flexural frame model resembles well the salient features of hysteretic response of column 2CMH18 up to the onset of shear failure ($\Delta_u^{Exp} = 28.0$ mm) but fails to detect the column shear failure. Therefore, the failure mode of column 2CMH18 would not have been in shear had the flexural model been employed.

Figure 17 demonstrates the hysteretic shear responses at various positions along the column height (Section I, II, III, and IV) obtained with the proposed force-based frame model, superimposed with the hysteretic sectional shear responses obtained with sixteen displacement-based frame elements of Sae-Long et al. [13]. Comparison between sectional shear responses obtained with these two frame models confirms the accuracy of the proposed force-based frame model in representing the local (sectional) responses. Due to restrained conditions, plastic hinge can only form at each end column (Section I). As shown in Figure 17(a), the shear response at Section I drastically differs from shear responses at all other sections (Figure 17(b) - (d)) locating outside the plastic-hinge region due to the shear-flexure interaction. At Section I, the shear response starts to deviate from the undamaged envelope curve once the sectional curvature ductility μ_ψ attains its threshold value of 3 as dictated in the UCSD shear-strength model. On the other hand, Sections II - IV response cyclically with respect to the undamaged envelope curve and behave nearly identically. Even though all column sections are subjected to the same value of shear force as governed by the equilibrium condition, Section I experiences much larger shear strain and eventually fails in shear at the ultimate value of $\gamma_u = 12 \times 10^{-3}$.

6. Conclusion

A force-based frame model with inclusion of shear-flexure interaction for seismic analyses of non-ductile reinforced concrete (RC) columns was presented in this work. Model formulation was conducted within the framework of virtual force principle. The sectional force fields were related to the element force degrees of freedom through equilibrated force shape functions. The frame-section kinematics followed the Timoshenko-beam hypothesis. The proposed frame model was not subjected to the "shear-locking" problematic phenomenon since there was no need for displacement-field approximations in the model formulation, thus eliminating the problem of displacement-field inconsistency. To demonstrate the big picture of the force-based finite element formulation, the modified Tonti's diagram was presented. One-dimensional models incorporated into the fiber-section model were employed to describe hysteretic responses of concrete, steel, and sectional shear force. The so-called "modified Mergos-Kappos" interaction procedure was adopted to account for the sectional shear-strength degradation associated with the inelastic flexural deformation. Evolution of the sectional shear-strength degradation with the inelastic flexural deformation followed the UCSD shear-strength model. With respect to validity of the model, correlation studies between experimental and numerical responses of flexure-shear critical RC columns under cyclic loadings revealed that the proposed force-based frame model could resemble well the salient features of the experimental force-displacement responses including the general shape of hysteretic response, the amount of dissipated hysteretic energy, and the member capacity. Sectional shear failure subsequent to plastic-hinge formation can accurately be captured by the proposed force-based frame model. This shear-failure mode involving sectional shear deterioration and rapid increase of the sectional shear strain subsequent to the plastic-hinge formation complied well with experimental observation. When the numerical simulation was conducted using the flexural model, necessity of accounting for the shear-flexure interaction was further emphasized. With respect to efficiency of the model, comparisons between numerical results obtained with the proposed force-based frame model and the displacement-based frame model of Sae-Long et al. [13] showed that a relatively coarse mesh of four proposed force-based frame elements can accurately reproduce both global and local responses obtained with a fine mesh of sixteen displacement-based frame elements by Sae-Long et al. [13], thus confirming superiority of the proposed force-based model over the displacement-based model.

A step forward on this study is to extend the shear constitutive model for prediction of softening behaviors of non-ductile RC structures under cyclic loading. This concept will be of benefit to seismic analyses of existing RC frame buildings in the future.

Author Contributions

W. Sae-Long played a role in implementing the numerical model, gathering the experimental data, interpreting the numerical results, and partially writing the manuscript; S. Limkatanyu played a role in formulating the numerical model, collecting the experimental data, interpreting the numerical results and partially writing the manuscript; C. Hansapinyo played a role in discussing the numerical results and partially writing the manuscript; T. Imjai played a role in revising the manuscript; and M. Kwon played a role in interpreting the numerical results. The manuscript was written through the contribution of all authors. All authors discussed the results, reviewed and approved the final version of the manuscript.



Acknowledgments

Financial support of this work was provided by the Thailand Research Fund (TRF) under Grant RTA6280012 and by the National Research Foundation of Korea (NRF) funded by the Government of South Korea (Ministry of Science and ICT; MSIT) (No.2019R1A2C1003007). Special thanks go to a senior lecturer Mr. Wiwat Sutiwipakorn for reviewing and correcting the English of this paper.

Conflict of Interest

The authors declared no potential conflicts of interest with respect to the research, authorship and publication of this article.

Funding

Financial support of this work was provided by the Thailand Research Fund (TRF) under Grant RTA6280012 and by the National Research Foundation of Korea (NRF) funded by the Government of South Korea (Ministry of Science and ICT; MSIT) (No.2019R1A2C1003007).

References

- [1] Neville, A.M., Brooks, J.J., *Concrete Technology (2nd edition)*, Pearson Education, Canada, 2010.
- [2] Lynn, A.C., Moehle, J.P., Mahin, S.A., Holmes, W.T., Seismic evaluation of existing reinforced concrete building columns, *Earthquake Spectra*, 12(4), 1996, 715-739.
- [3] Moehle, J.P., Mahin, S.A., Observations on the behavior of reinforced concrete buildings during earthquakes, *ACI SP-127: Earthquake-Resistant Concrete Structures Inelastic Response and Design*, American Concrete Institute, Detroit, USA, 1991.
- [4] Aschheim, M., Gülkan, P., Sezen, H., Bruneau, M., Elnashai, A.S., Halling, M., Love, J., Rahnama, M., Performance of buildings, *Earthquake Spectra*, 16(S1), 2000, 237-279.
- [5] Sezen, H., Whittaker, A.S., Elwood, K.J., Mosalam, K.M., Performance of reinforced concrete buildings during the August 17, 1999 Kocaeli, Turkey earthquake, and seismic design and construction practice in Turkey, *Engineering Structures*, 25(1), 2003, 103-114.
- [6] Lukkunaprasit, P., Ruangrassamee, A., Boonyatee, T., Chintanapakdee, C., Jankaew, K., Thanasisathit, N., Chandrangsu, T., Performance of structures in the Mw 6.1 Mae Lao Earthquake in Thailand on May 5, 2014 and implications for future construction, *Journal of Earthquake Engineering*, 20(2), 2015, 219-242.
- [7] Lynn, A.C., Seismic evaluation of existing reinforced concrete building columns, Ph.D. Thesis, Department of Civil and Environmental Engineering, University of California, Berkeley, USA., 2001.
- [8] Elwood, K.J., Modelling failures in existing reinforced concrete columns, *Canadian Journal of Civil Engineering*, 31(5), 2004, 846-859.
- [9] Sezen, H., Moehle, J.P., Seismic test of concrete columns with light transverse reinforcement, *ACI Structural Journal*, 103(6), 2006, 842-849.
- [10] Lodhi, M.S., Sezen, H., Estimation of monotonic behavior of reinforced concrete columns considering shear-flexure-axial load interaction, *Earthquake Engineering & Structural Dynamics*, 41(15), 2012, 2159-2175.
- [11] Vecchio, C.D., Kwon, O.S., Sarno, L.D., Prota, A., Accuracy of nonlinear static procedures for the seismic assessment of shear critical structures, *Earthquake Engineering & Structural Dynamics*, 44(10), 2015, 1581-1600.
- [12] Zimos, D.F., Modelling the post-peak response of existing reinforced concrete frame structures subjected to seismic loading, Ph.D. Thesis, Computer Science and Engineering, Research Centre for Civil Engineering Structures, University of London, England, 2017.
- [13] Sae-Long, W., Limkatanyu, S., Prachasaree, W., Horpibulsuk, S., Panedpojaman, P., Nonlinear frame element with shear-flexure interaction for seismic analysis of non-ductile reinforced concrete columns, *International Journal of Concrete Structures and Materials*, 13, Article number: 32, 2019.
- [14] Ozcebe, G., Saatcioglu, M., Hysteretic shear model for reinforced concrete members, *Journal of Structural Engineering*, 115(1), 1989, 132-148.
- [15] Sezen, H., Seismic behavior and modeling of reinforced concrete building columns, Ph.D. Thesis, Department of Civil and Environmental Engineering, University of California, Berkeley, USA., 2002.
- [16] Lee, J.Y., Watanabe, F., Predicting the longitudinal axial strain in the plastic hinge regions of reinforced concrete beams subjected to reversed cyclic loading, *Engineering Structures*, 25(7), 2003, 927-939.
- [17] Biskinis, D., Roupakias, G.K., Fardis, M.N., Degradation of shear strength of reinforced concrete members with inelastic cyclic displacement, *ACI Structural Journal*, 101(6), 2004, 773-783.
- [18] Priestley, M.J.N., Seible, F., Verma, R., Xiao, Y., Seismic shear strength of reinforced concrete columns, *Structural Systems Research Project Report No. SSRP 93/06*, University of California, San Diego, USA, 1993.
- [19] Sezen, H., Moehle, J.P., Shear strength model for lightly reinforced concrete columns, *Journal of Structural Engineering*, 130(11), 2004, 1692-1703.
- [20] ICC, International building code, *International Code Council*, Country Club Hills, Illinois, USA., 2012.
- [21] Ceresa, P., Petrini, L., Pinho, R., Flexure-shear fiber beam-column elements for modeling frame structures under seismic loading: State of the art, *Journal of Earthquake Engineering*, 11(supplement 1), 2007, 46-88.
- [22] Ceresa, P., Petrini, L., Pinho, R., A fiber flexure-shear model for cyclic nonlinear behavior of RC structural elements, *Research Report ROSE-2008/07*. IUSS Press: Pavia, Italy, 2008.
- [23] Giberson, M.F., The response of nonlinear multi-story structures subjected to earthquake excitation, *Earthquake Engineering Research Laboratory*, California Institute of Technology, Pasadena, USA, 1967.
- [24] Roufaiel, M.S.L., Meyer, C., Analytical modeling of hysteretic behavior of R/C frames, *Journal of Structural Engineering*, 113(3), 1987, 429-444.
- [25] Thom, C., The effects of inelastic shear on the seismic response of structures, Ph.D. Thesis, University of Auckland, New Zealand, 1983.
- [26] Pincheira, J.A., Dotiwala, F.S., D'Souza, J.T., Seismic analysis of older reinforced concrete columns, *Earthquake Spectra*, 15(2), 1999, 245-272.
- [27] Sezen, H., Chowdhury, T., Hysteretic model for reinforced concrete columns including the effect of shear and axial load failure, *Journal of Structural Engineering*, 135(2), 2009, 139-146.
- [28] Soleimani, D., Reinforced concrete ductile frames under earthquake loadings with stiffness degradation, Ph.D. Thesis, University of California, Berkeley, USA., 1978.
- [29] Lee, C., Filippou, F., Efficient beam-column element with variable inelastic end zones, *Journal of Structural Engineering*, 135(11), 2009, 1310-1319.
- [30] Mullapudi, T.R., Ayoub, A., Modeling of the seismic behavior of shear-critical reinforced concrete columns, *Engineering Structures*, 32(11), 2010, 3601-3615.
- [31] Guner, S., Vecchio, F.J., Simplified method for nonlinear dynamic analysis of shear-critical frames, *ACI Structural Journal*, 109(5), 2012, 727-738.
- [32] Mergos, P.E., Kappos, A.J., A gradual spread inelasticity model for R/C beam-columns, accounting for flexure, shear and anchorage slip, *Engineering Structures*, 44, 2012, 94-106.
- [33] Mergos, P.E., Kappos, A.J., A distributed shear and flexural flexibility model with shear-flexure interaction for R/C members subjected to seismic loading, *Earthquake Engineering & Structural Dynamics*, 37(12), 2008, 1349-1370.
- [34] Zimos, D.K., Mergos, P.E., Kappos, A.J., Modelling of R/C members accounting for shear failure localisation: Hysteretic shear model, *Earthquake Engineering & Structural Dynamics*, 47(8), 2018, 1722-1741.
- [35] Zeris, C.A., Mahin, S.A., Behavior of reinforced concrete structures subjected to uniaxial excitation, *Journal of Structural Engineering*, 117(9), 1991, 2657-2673.
- [36] Spacone, E., Filippou, F.C., Taucer, F.F., Fibre beam-column model for nonlinear analysis of R/C frames. Part I: formulation, *Earthquake Engineering & Structural Dynamics*, 25(7), 1996, 711-725.



- [37] Spacone, E., Limkatanyu, S., Responses of reinforced concrete members including bond-slip effects, *ACI Structural Journal*, 97(6), 2000, 831-839.
- [38] Cosenza, E., Manfredi, G., Verderame, G.M., A fibre model for push-over analysis of underdesigned reinforced concrete frames, *Computers & Structures*, 2006, 84(13-14), 904-916.
- [39] Marini, A., Spacone, E., Analysis of reinforced concrete elements including shear effects, *ACI Structural Journal*, 103(5), 2006, 645-655.
- [40] Ceresa, P., Petrini, L., Pinho, R., Sousa, R., A fibre flexure-shear model for seismic analysis of RC-framed structures, *Earthquake Engineering & Structural Dynamics*, 38(5), 2009, 565-586.
- [41] Palermo, D., Vecchio, F.J., Compression field modeling of reinforced concrete subjected to reversed loading: Formulation, *ACI Structural Journal*, 100(5), 2003, 616-625.
- [42] Hsu, T.T.C., Zhu, R.R.H., Softened membrane model for reinforced concrete elements in shear, *ACI Structural Journal*, 99(4), 2002, 460-469.
- [43] Feng, D.C., Wu, G., Sun, Z.Y., Xu, J.G., A flexure-shear Timoshenko fiber beam element based on softened damage-plasticity model, *Engineering Structures*, 140, 2017, 483-497.
- [44] Wu, J.Y., Li, J., Faria, R., An energy release rate-based plastic-damage model for concrete, *International Journal of Solids and Structures*, 43(3-4), 2006, 583-612.
- [45] Feng, D.C., Wu, G., Ning, C.L., A regularized force-based Timoshenko fiber element including flexure-shear interaction for cyclic analysis of RC structures, *International Journal of Mechanical Sciences*, 160, 2019, 59-74.
- [46] Limkatanyu, S., Spacone, E., Reinforced concrete frame element with bond interfaces. I: Displacement-based, force-based, and mixed formulations, *Journal of Structural Engineering*, 128(3), 2002, 346-355.
- [47] Jafari, V., Abyaneh, M.A., Vahdani, S.H., Rahimian, M., Improved displacement-field approximation for geometrical nonlinear flexibility-based planar curved element in state space, *Mechanics Based Design of Structures and Machines*, 37(4), 2009, 475-502.
- [48] Zendaoui, A., Kadid, A., Yahiaoui, D., Comparison of different numerical models of RC elements for predicting the seismic performance of structures, *International Journal of Concrete Structures and Materials*, 10(4), 2016, 461-478.
- [49] Tonti, E., The reason for analogies between physical theories, *Applied Mathematical Modelling*, 1(1), 1976, 37-50.
- [50] Taylor, R.L., FEAP: A finite element analysis program, *User manual: version 7.3. Department of Civil and Environmental Engineering*, University of California, Berkeley, USA, 2000.
- [51] Onate, E., *Structural analysis with the finite element method volume 2: beams, plates and shells*, Springer, Netherlands, 2013.
- [52] Kent, D.C., Park, R., Flexural members with confined concrete, *ASCE Journal of the Structural Division*, 97(7), 1971, 1969-1990.
- [53] Menegotto, M., Pinto, P.E., Method of analysis for cyclically loaded reinforced concrete plane frames including changes in geometry and nonelastic behavior of elements under combined normal force and bending, *Proceeding of IABSE Symposium on Resistance and Ultimate Deformability of Structures Acted on by Well-Defined Repeated Loads*, Lisbon, 1973, 15-22.
- [54] Spacone, E., Filippou, F.C., Taucer, F.F., Fibre beam-column model for nonlinear analysis of R/C frames. Part II: Applications, *Earthquake Engineering & Structural Dynamics*, 25(7), 1996, 727-742.
- [55] Limkatanyu, S., Spacone, E., Reinforced concrete frame element with bond interfaces. II: State determinations and numerical validation, *Journal of Structural Engineering*, 128(3), 2002, 356-364.
- [56] Park, R., Paulay, T., *Reinforced concrete structures*, John Wiley & Sons, New York, USA, 1975.
- [57] Ma, S.M., Bertero, V.V., Popov, E.P., Experimental and analytical studies on hysteretic behavior of RC rectangular and T-beam, *Earthquake Engineering Research Center Report No. UCB/EERC-76/02*, University of California, Berkeley, USA, 1976.
- [58] Oosterle, R.G., Fiorato, A.E., Aristizabal-Ochoa, J.D., Corley, W., Hysteretic response of reinforced concrete structural walls, In: *Proceedings of ACISP-63: reinforced concrete structures subjected to wind and earthquake forces*, Detroit, USA, 1980.
- [59] Ramirez, H., Jirsa, J.O., Effect of axial load on shear behavior of short RC columns under cyclic lateral deformations, *PMFSEL REPORT No. 80-1*, Phil M. Ferguson Structural Engineering Laboratory, Department of Civil Engineering, The University of Texas at Austin, USA., 1980.
- [60] Sezen, H., Shear deformation model for reinforced concrete columns, *Structural Engineering & Mechanics*, 28(1), 2008, 39-52.
- [61] Li, Z.X., Gao, Y., Zhao, Q., A 3D flexure-shear fiber element for modeling the seismic behavior of reinforced concrete columns, *Engineering Structures*, 117, 2016, 372-383.
- [62] Filippou, F.C., D'Ambrisi, A., Issa, A., Nonlinear static and dynamic analysis of reinforced concrete subassemblages, *Earthquake Engineering Research Center Report No. UCB/EERC-92/08*, University of California, Berkeley, USA, 1992.
- [63] Martino, R., Nonlinear pushover analysis of reinforced concrete structures, Master Thesis, Department of Civil, Environmental, Architectural Engineering, University of Colorado, Boulder, USA, 1999.

ORCID iD

Worathep Sae-Long  <https://orcid.org/0000-0001-8149-4409>
 Suchart Limkatanyu  <https://orcid.org/0000-0002-4343-7654>
 Chayanon Hansapinyo  <https://orcid.org/0000-0002-6237-613X>
 Thanongsak Imjai  <https://orcid.org/0000-0002-3220-7669>
 Minh Kwon  <https://orcid.org/0000-0003-0754-285X>



© 2020 by the authors. Licensee SCU, Ahvaz, Iran. This article is an open access article distributed under the terms and conditions of the Creative Commons Attribution-NonCommercial 4.0 International (CC BY-NC 4.0 license) (<http://creativecommons.org/licenses/by-nc/4.0/>).

How to cite this article: Sae-Long W., Limkatanyu S., Hansapinyo C., Imjai T., Kwon M. Forced-based Shear-flexure-interaction Frame Element for Nonlinear Analysis of Non-ductile Reinforced Concrete Columns, *J. Appl. Comput. Mech.*, 6(SI), 2020, 1151-1167. <https://doi.org/10.22055/JACM.2020.32731.2065>

